Supporting Materials

The small molecule inhibitor NAV-2729 has a complex target profile including multiple ADP-ribosylation factor regulatory proteins

Eric M. Rosenberg Jr.[1,†], Xiaoying Jian[1,†], Olivier Soubias[2], Hye-Young Yoon[1], Mukesh P. Yadav[1,‡], Sarah Hammoudeh[1], Sandeep Pallikkuth[1], Itoro Akpan[1], Pei-Wen Chen[3], Tapan K. Maity[4], Lisa M. Jenkins[4], Marielle E. Yohe[5,6], R. Andrew Byrd[2], Paul A. Randazzo[1]*

Affiliations:

[1]Laboratory of Cellular and Molecular Biology, Center for Cancer Research, National Cancer Institute; Bethesda, MD, USA.

[2]Center for Structural Biology Laboratory, Center for Cancer Research, National Cancer Institute; Frederick, MD, USA.

[3]Department of Biology, Williams College; Williamstown, MA, USA.

[4]Laboratory of Cell Biology, Center for Cancer Research, National Cancer Institute; Bethesda, MD, USA.

[5]Pediatric Oncology Branch, Center for Cancer Research, National Cancer Institute; Bethesda, MD, USA.

[6]Laboratory of Cell and Developmental Signaling, Center for Cancer Research; Frederick, MD, USA.

*Corresponding author. Email: randazzp@mail.nih.gov

† These authors contributed equally to this work

‡ Current address: University of Maryland School of Medicine, Department of Diagnostic Radiology; Baltimore, MD, USA.

Supporting results

Determination of optical and physical properties of NAV-2729

To guide biochemical studies, we examined the physical and optical properties of NAV-2729 in aqueous solution (phosphate buffered saline, PBS) and in dimethylsulfoxide (DMSO). In

PBS, NAV-2729 had an absorption peak at ~312 nm with a shoulder at 408nm and a molar absorbance coefficient of 16,000 OD/M/cm at 320. In DMSO, NAV-2729 had an absorption peak at 280 nm (Supplemental Fig. S1A). The molar absorbance coefficient at 280 nm was 29,000 OD/M/cm. In both PBS and DMSO, peak absorption was linear with concentration to 25 μM NAV-2729 (Supplemental Fig. S1B).

NAV-2729 had no detectable fluorescence but scattered light when in aqueous solution. In initial experiments, NAV-2729 in PBS containing 0.1% DMSO was excited with 290 nm light and emission from 305 to 650 nm was measured. There was a sharp peak at 590 nm (Supplemental Fig. S1C). The spectrum was otherwise flat. The peak observed at 590 nm was likely second-order scatter (Supplemental Fig. S1C), a phenomenon in which the incident light is first scattered in solution and subsequently diffracted after reaching the emission monochromator of the fluorescence spectrometer, thus being detected at double the excitation wavelength (77). With incident light of 280 and 330 nm, similar sharp peaks were observed at approximately 560 and 660 nm (Supplemental Fig. S1D). When the wavelength of incident light was varied from 200 to 400 nm while detecting emission at 590 nm, a sharp peak at 295 nm was observed (Supplemental Fig. S1E). With incident light at 290 nm, the height of the peak at 582 nm was linearly related to NAV-2729 concentration from 0.2 to 2.5 μM (Supplemental Fig. S1F). Taken together, these results are consistent with second-order scattering. In DMSO, a small peak of fluorescence, probably from DMSO, was observed (Supplemental Fig. S1C). Less second-order scatter was detected in DMSO than in PBS (Supplemental Fig. S1C), which was not related to NAV-2729 concentration (Supplemental Fig. S1G; the spectra used for Fig. S1G was obtained with an emission slit of 5 nm to increase signal, whereas in the other spectra presented both excitation and emission slits were 2.5 nm). NAV-2729, at 25 μM, quenched fluorescence from DMSO (Supplemental Fig. S1H,

spectra obtained with a 5 nm emission slit). 200 μM of a phospholipid analog with octanoic acid side chains, dioctanoyl phosphatidylinositol 4,5-bisphosphate (diC8-PIP2), which has a predicted critical micellar concentration of greater than 3 mM (78), did not affect NAV-2729 light scattering (Supplemental Fig. S1I).

Light scattering was consistent with the idea that NAV-2729 forms supramolecular assemblies in solution. Negative stain electron microscopy was used to directly image the assemblies at [NAV-2729] = 25 and 50 μM, as well as a control solution of 0.5% DMSO in PBS (Supplemental Fig. S2A). In the images of the control (i.e., no NAV-2729), no consistent structures were identified; however, at 25 and 50 μM NAV-2729, spherical structures were observed (Supplemental Fig. S2A). The average diameter of the structures increased with NAV-2729 concentration, with the median average diameter at 25 μM and 50 μM NAV-2729 being 51 and 106 nm (Supplemental Fig. S2B). Using polypropylene centrifuge tubes (NAV-2729 adsorbs quantitatively to polycarbonates, see below), we observed that the NAV-2729 structures could be precipitated from solution. While variable between experiments, we observed that approximately 20% and 30% of the NAV-2729 at concentrations of 25 and 50 μM could be recovered in the pellet with this method (Supplemental Fig. S2C).

The proton NMR spectrum of NAV-2729 was also examined. NMR signals were not observed in aqueous solution, while a well resolved spectrum was observed in DMSO (former not shown; see Supplemental Fig. S3H for the latter). Four observations—first, light scattering when in PBS but not in DMSO (Supplemental Fig. S1C); second, visible particles seen in negative stain electron microscopy (Supplemental Fig. S2A); third, NAV-2729 pelleting when centrifuged (Supplemental Fig. S2C); and fourth, lack of proton NMR signal in aqueous solution but a well

resolved spectrum in DMSO (data not shown and Supplemental Fig. S2D)—taken together, support the idea that NAV-2729 forms supramolecular assemblies in aqueous solution.

Partitioning into LUVs was tested by other methods. NAV-2729 does not adsorb to the same extent to polypropylene as to polycarbonate, but does precipitate in the centrifugal field, which was used to determine binding to protein (as described in main text). We used the property of adsorption to polycarbonate in a test for partitioning into LUVs. 25 μM NAV-2729 was incubated with sucrose-loaded LUVs at a total phospholipid concentration of 0.5 mM. The LUVs were separated from the bulk solution by centrifugation. Approximately 80% of the NAV-2729 was recovered in the pellet with the LUVs. Without LUVs, NAV-2729 quantitatively adsorbed to the polycarbonate tubes and was not recovered (Supplemental Fig. S3A). In another approach to determine if NAV-2729 partitioned into LUVs, the effect of LUVs on the UV/VIS spectrum of NAV-2729 was determined (Supplemental Fig. S3B). LUVs were titrated from 0.1 mM to 0.5 mM total phospholipid concentration into a solution with 25 μM NAV-2729. Without LUVs, absorbance peaked at 310 – 320 nm with a shoulder at 408 nm. In the presence of LUVs, there was an increase absorbance at 312 nm and a decrease at 408 nm (Supplemental Fig. S3B). This difference in absorbance was a function of LUV concentration (Supplemental Fig. S3C).

As an additional test of partitioning into LUVs, LUVs with and without NAV-2729 were visualized by negative stain electron microscopy (Supplemental Fig. S3D). LUVs in the absence of NAV-2729 were largely spherical with a median average diameter of 103.3 nm (Supplemental Fig. S3E). As described above, NAV-2729 at a concentration of 50 μM formed assemblies in the same size range but with distinct morphology. When combined with LUVs, the spherical structures apparent with NAV-2729 alone (Supplemental Fig. S2A) were absent, indicating NAV-2729 had combined with the LUVs (Supplemental Fig. S2A, S3D). Further, at a concentration of

25 μM NAV-2729 incubated with LUVs, the median average diameter of the particles, 100.1 nm, was nearly identical to LUVs without NAV-2729 (Supplemental Fig. S3E). There were insufficient images of LUVs with 50 μM NAV-2729 to determine if the average particle diameter was different from controls (data not shown). Using polypropylene tubes and a fixed concentration of sucrose-loaded LUVs, we observed that the amount of NAV-2729 recovered after centrifugation was linearly related to the amount of NAV-2729 added to the LUVs, with approximately 86% being recovered at any given concentration (Supplemental Figure S3F). These results suggested that most of the NAV-2729 partitions into LUVs using this method, which was later used to measure protein binding (as described in main text).

An additional observation was that NAV-2729 quenched signal from a membrane marker, indicating incorporation into membranes (Supplemental Fig. S3G). RD cells were treated with NAV-2729 or Bragsin, fixed and stained with the membrane marker MemGlow 560 (Cytoskeleton), which is incorporated into cell membranes and contains the fluorophore Alexa560. In the control cells and cells treated with Bragsin, fluorescence was greater in the cells than the background (Supplemental Fig. S3G). In cells treated with NAV-2729, no signal was observed. When the exposure was increased to reveal background, the cells were observed as objects with less signal than the background (Supplemental Fig. S3G).

NMR was also used to examine the effect of introducing NAV-2729 to lipid membranes. The proton spectrum of NAV-2729 dissolved in DMSO allowed for identification of ^{1}H peaks corresponding to NAV-2729, including protons associated with aromatic groups (Supplemental Fig. S3H, bottom). Nanodiscs (NDs) were used to mimic a lipid membrane, and when introduced to aqueous solution several peaks corresponding to the ND belt proteins and phospholipids could be observed (Supplemental Fig. S3H, top). The NDs were mixed with NAV-2729 in a 1:1

stoichiometric ratio in aqueous solution. While many of the peaks from NAV-2729 were obscured by the spectrum of the NDs, the peaks corresponding to the aromatic protons from NAV-2729 could be resolved. (Supplemental Fig. S3H, middle). These results support the idea that NAV-2729 partitions into phospholipid membranes in aqueous solution.

Supporting experiment procedures

Measurement of fluorescence and scatter: A Horiba FluoroMax-3 was used to irradiate samples with UV/Vis light and determine signal at 90° from the incident light. Solvent, NAV-2729 concentration, and wavelengths of incident light and emitted light, as well as the slits widths used are indicated in the figure legends.

UV/VIS spectrometry: Spectra were obtained with a Perkin Elmer Lambda 25 and a Perkin Elmer Lambda 265. Baselines were established using the buffer and all additions but without NAV-2729. For example, for spectra obtained with LUVs, baselines were established with LUVs in the absence of NAV-2729.

Electron microscopy: 25 mM NAV-2729, dissolved in DMSO, was diluted to 12.5 mM in DMSO, and these two solutions provided 500x stocks for the assay. The 500x stocks (or pure DMSO) were then diluted 1:450 by addition of 1x PBS supplemented with 0.334% DMSO, yielding solutions at 1.11x concentration. 90 μL of the 1.11x stocks were then added to microcentrifuge tubes, one set to examine NAV-2729 supramolecular assemblies and the other set to examine NAV-2729 mixed with LUVs. To the former set, 10 μL of 1x PBS was added to the 1.11x stocks; to the latter set, 10 μL of a 5 mM LUV solution was added to the 1.11x stocks. The final concentrations of each solution were 0, 25, or 50 μM NAV-2729, 500 μM LUVs (only in the LUV set), and 0.5% DMSO. The reactions were incubated for 5 min. at room temperature, after which they were stored at 4°C until being used for negative stain electron microscopy. Negative stains were performed as a fee-

for-service at the National Cancer Institute Center for Cancer Research (NCI CCR) Electron Microscopy Lab located in Frederick, Maryland using a Hitachi H-7600 transmission electron microscope at 20,000, 25,000, and 30,000x magnification. Size analysis was performed by measuring the individual diameters of NAV-2729 supramolecular assemblies and LUVs based on pixel size (in units of nm/pixel), and the average diameters were used for plotting and statistical analysis.

Supplemental Fig. S1. **Optical properties of NAV-2729.** (**A**) UV/VIS absorbance spectrum dependence on solvent. NAV-2729 was dissolved in either DMSO or PBS containing 0.1% DMSO with a final concentration of 25 μM. An absorption spectrum was determined with a Perkin Elmer Lambda 25 using a quartz cuvette with a 1 cm path length. (**B**) Effect of solvents and lipids on NAV-2729 optical absorption. Absorption at the absorption peak in either DMSO, PBS with 0.1% DMSO, or PBS with 0.1% DMSO and LUVs (total phospholipid concentration of 250 μM) was determined for the indicated concentrations of NAV-2729 in quartz cuvette with a 1 cm path. (**C**) Emission spectra of NAV-2729 in the indicated solvent and excited with 290 nm light. (**D**) Emission spectra of NAV-2729 in PBS with 0.1% DMSO excited with light at the indicated wavelengths. (**E**) Excitation spectrum of NAV-2729 in PBS with 0.1% DMSO with emission at 582 nm. (**F**) NAV-2729 concentration dependence of 582 nm emission with 290 nm excitation with NAV-2729 in PBS with 0.1% DMSO. (**G**) NAV-2729 concentration dependence of 582 nm emission when NAV-2729 is in DMSO. (**H**) Effect of NAV-2729 on emission spectrum of DMSO with 290 nm incident light. (**I**) Effect of dioctanoyl PIP2 (diC8-PIP2) on 582 emission observed with NAV-2729 in PBS and 290 nm incident light.

Supplemental Fig. S2. **NAV-2729 forms supramolecular assemblies.** (**A**) Negative stain images of PBS supplemented with 0.5% DMSO alone and with 25 or 50 μM NAV-2729. Scale bars are

100 nms in length. (**B**) Quantification of the sizes of the particles of NAV-2729 shown in (A). Medians are shown as a line. The difference in average diameter was determined to be significantly different (****, $p < 0.0001$) via an unpaired t-test with Welch's correction. (**C**) Recovery of NAV-2729 by centrifugation. NAV-2729 at the indicated concentrations in aqueous solution was subject to a 250,000 *g* centrifugal field. The supernatant was aspirated and sedimented material was resuspended in PBS. NAV-2729 concentration was determined by UV/Vis absorption spectrometry.

Supplemental Fig. S3. **NAV-2729 partitions into membranes.** (**A**) Recovery of NAV-2729 in LUVs. 25 μM NAV-2729 was incubated in PBS with 0.1% DMSO and 0.5 mM LUVs where indicated in polycarbonate centrifuge tubes. The mixtures were subject to a 250,000 *g* centrifugal field at 4°C for 15 min. and solution was removed from the tubes. Any sedimented material was resuspended in PBS with 0.1% PBS and UV/VIS spectra of the starting mixtures, supernatant and pelleted materials were measured to determine NAV-2729 mass in each. (**B**) Difference in NAV-2729 spectra obtained in PBS with 0.1% DMSO with and without LUVs. (**C**) Effect of LUVs on the spectrum of NAV-2729. LUVs were titrated into a mixture of NAV-2729 in PBS with 0.1% DMSO. UV/VIS spectra were measured. The ratio of the peak height at 312 nm to peak height at 408 nm is plotted against LUV concentration, the latter reported as total phospholipid concentration. (**D**) Negative stain images of 500 μM LUVs in PBS supplemented with 0.5% DMSO, either alone or with 25 or 50 μM NAV-2729. (**E**) Quantification of the sizes of the LUVs shown in (D). Medians are shown as a line. ns, not significant as determined via an unpaired t-test with Welch's correction. Scale bars are 100 nms in length. (**F**) Fraction of NAV-2729 recovered in LUVs. NAV-2729 was incubated at the indicated concentrations in a mixture of PBS with 0.5% DMSO and sucrose-loaded LUVs (containing a total of 500 μM phospholipids). The LUVs were

collected by centrifugation and recovered NAV-2729 was determined by UV/VIS absorption spectrometry. Recovered NAV-2729 is plotted against the starting concentration. (**G**) NAV-2729 quenches signal of fluorescent membrane marker. RD cells were plated on fibronectin-coated coverslips, treated for 2 hrs with the indicated compound and then fixed with paraformaldehyde prior to staining with Memglo™560 (Cytoskeleton). Fluorescent signal was imaged with a Zeiss epifluorescent microscope. The images for the top two panels and the lower left panel were taken at the same exposure. Exposure time was increase 8-fold for the image in the lower right panel to increase the background signal, revealing absence of signal in the place of cells. The scale bars are 100 μms in length. (**H**) Proton spectra of NAV-2729 in DMSO as well as nanodiscs in aqueous solution with and without NAV-2729. *Top*. Nanodiscs in aqueous solution (ND^{H_2O}). Peaks correspond to those from the NANODISC lipids and belt proteins. *Middle*. nanodiscs in aqueous solution mixed with NAV-2729 (ND^{H_2O}:NAV). Peaks with asterisks correspond to those from NAV-2729. *Bottom*. NAV-2729 in DMSO. Distinct peaks from NAV-2729 can be observed.

Supplemental Fig. S4. **Biochemical characterization of NAV-2729 effects on recombinant ASAP1.** (**A**) NAV-2729 inhibits the Arf GAP activity of full-length ASAP1. For this assay, myrArf1 was used as a substrate on LUVs containing PIP2. Image is a representative example of 4 experiments. **(B**) Preliminary experiment showing that ASAP1 no longer relies on NAV-2729 for cosedimentation with LUVs at high PIP2 concentrations. A construct encoding the PH, Arf GAP, and ankyrin repeats (PZA construct) of ASAP1 was tested for binding as described in Fig. 4C. For this assay, LUVs containing 2.5% PIP2 were used. Top image shows gel results of experiment while the bottom shows the quantified data. (**C**) NAV-2729 inhibits ASAP1 PZA using [L8K]Arf1 as a substrate in conditions with LUVs (2.5% PIP2). Image is a representative example of 4 experiments. (**D**) ASAP1 PZA in thermostabilized at 51°C as a function of NAV-2729

concentration. Top image shows gel results of experiment while the bottom shows the quantified data. Image is a representative example of 2 experiments. (**E**) NAV-2729 alters the dependence of ASAP1 on PIP2 for GAP activity. GAP assays were conducted as described in Fig. 6A. Reactions using myrArf1 as a substrate were conducted with LUVs containing increasing amounts of PIP2. Image is representative of 3 experiments. (**F**) Same as (E), except assays were conducted with soluble diC8-PIP2 rather than LUVs containing PIP2, and [L8K]Arf1 as a substrate rather than myrArf1. Image is representative of 4 experiments.

Supplemental Table S1. **Cellular Thermal Shift Assay screen for proteins that bind NAV-2729.** RD cell lysates were mixed with DMSO or 50 μM NAV-2729 and subjected to a temperature ramp. The lysates were centrifuged and the proteins remaining in solution were detected by mass spectrometry. The data were then analyzed to determine temperature shifts as described in "Materials and Methods." 19 of the 25 proteins determined to have a significant negative temperature shift bound to nucleotide or nucleic acid. 8 of 20 with a positive shift bound to nucleotide or nucleic acid.

References:

77. Lakowicz, J. R. (2006) *Principles of fluorescence spectroscopy*, Springer

78. Senning, E. N., Collins, M. D., Stratiievska, A., Ufret-Vincenty, C. A., and Gordon, S. E. (2014) Regulation of TRPV1 ion channel by phosphoinositide (4,5)-bisphosphate: the role of membrane asymmetry. *The Journal of biological chemistry* **289**, 10999-11006

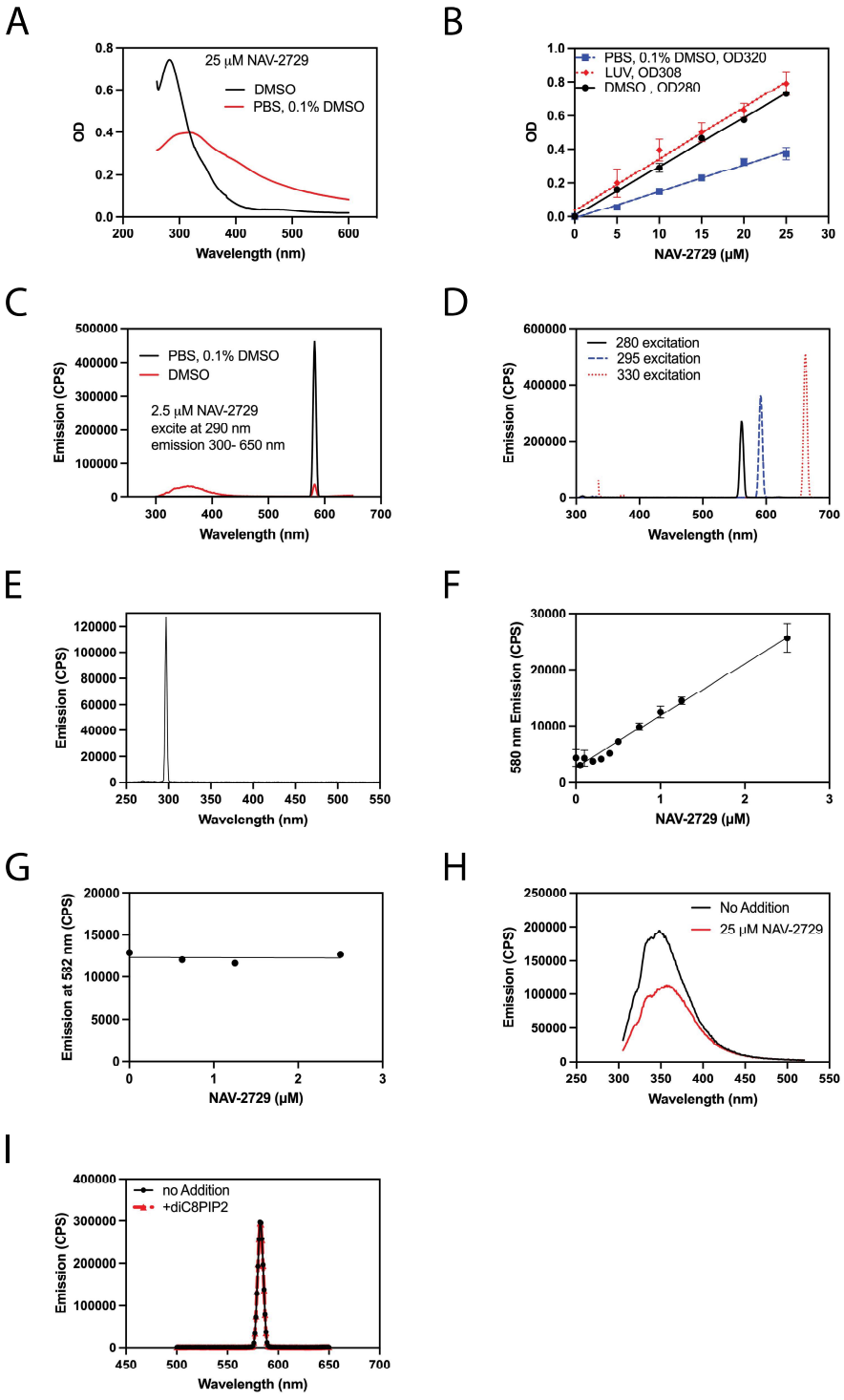

Supplemental Figure S1. Rosenberg, Jian, et al.

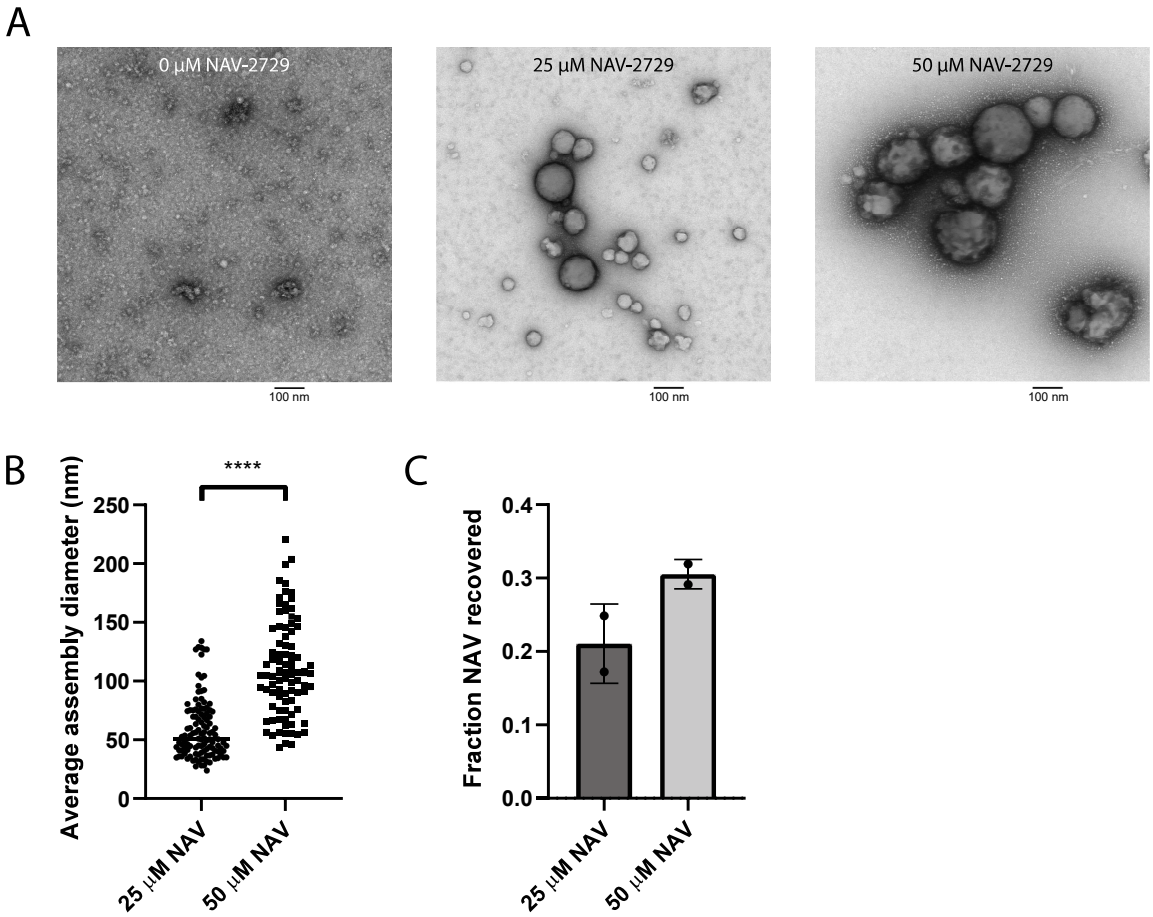

Supplemental Figure S2. Rosenberg, Jian, et al.

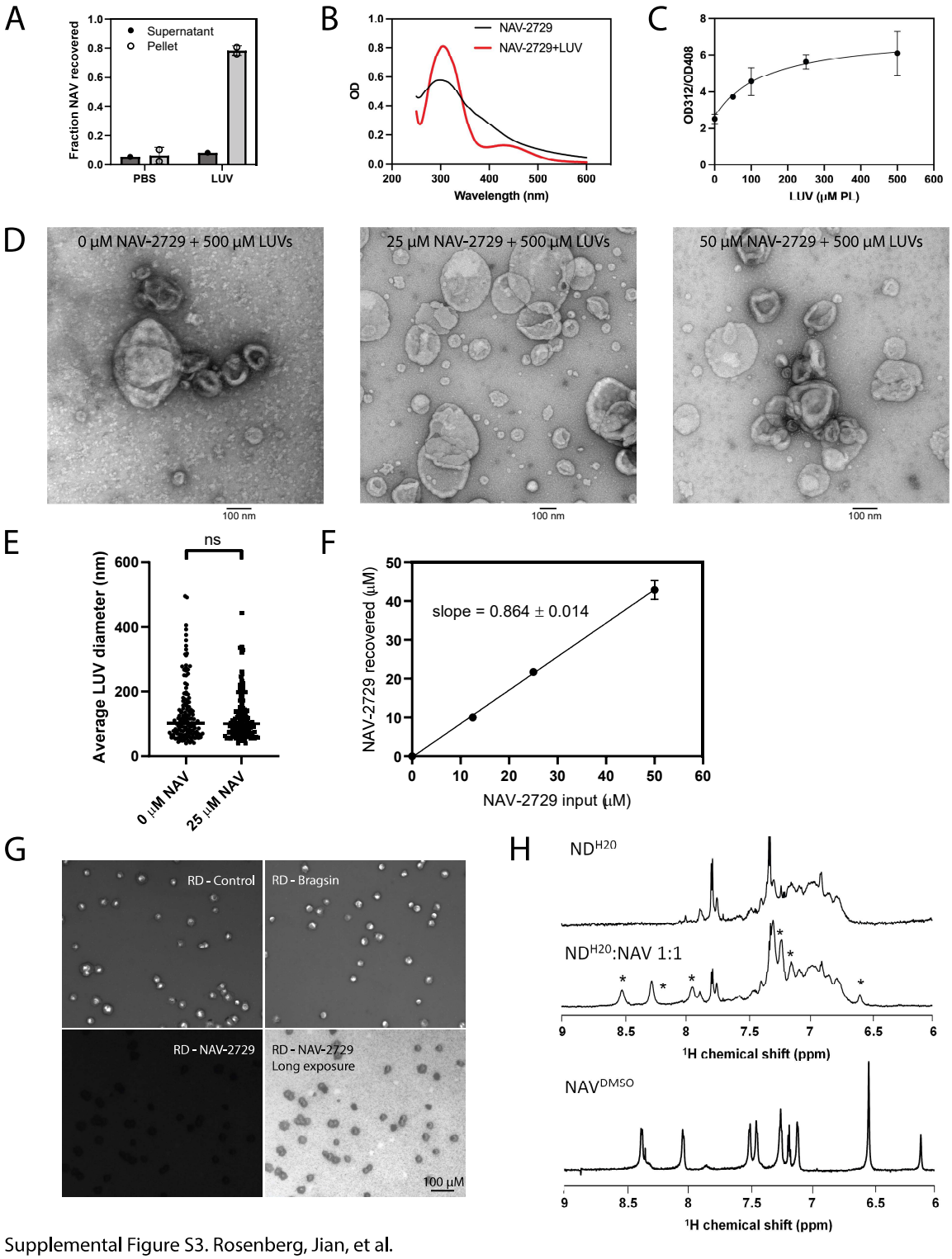

Supplemental Figure S3. Rosenberg, Jian, et al.

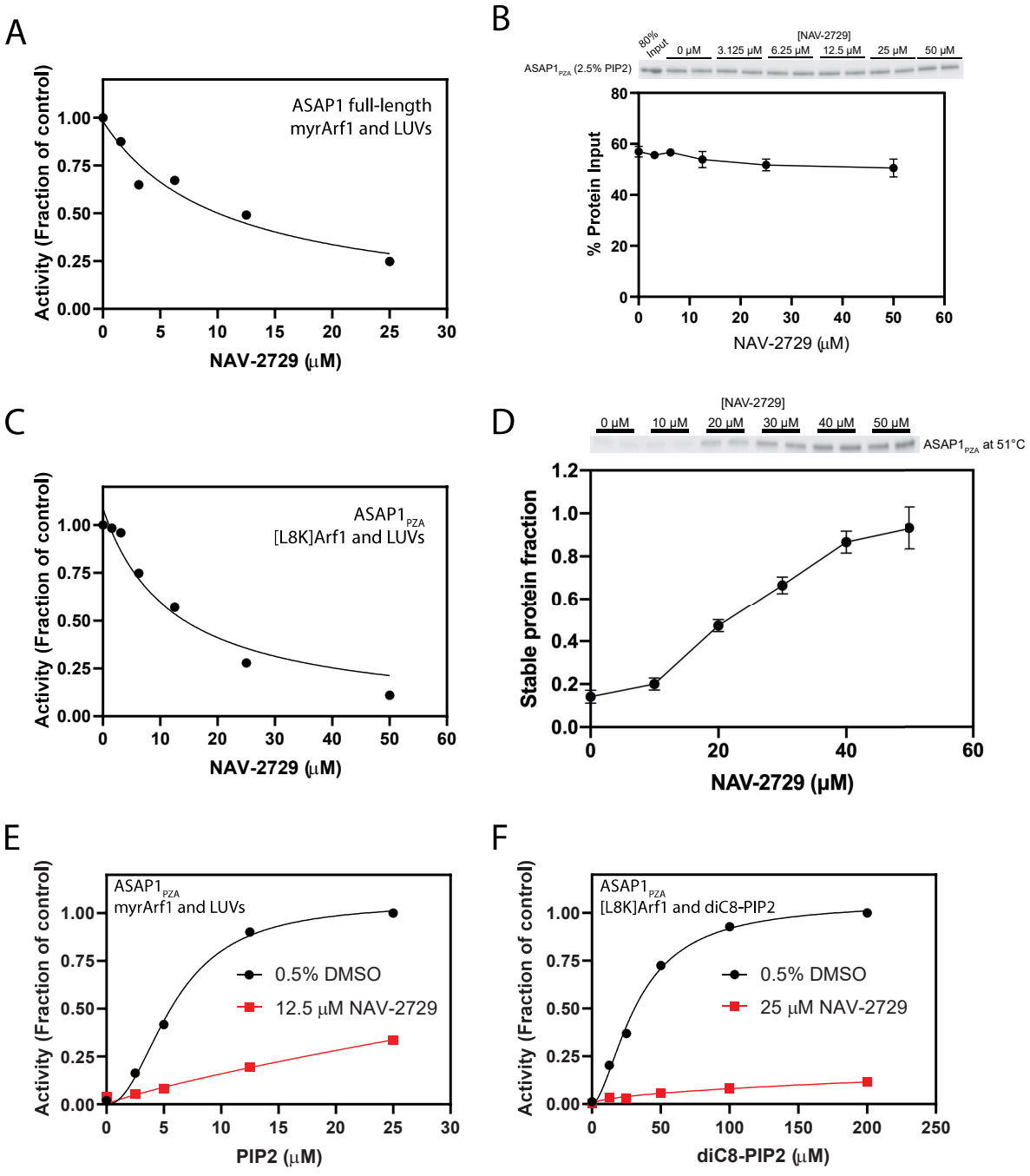

Figure S4. Rosenberg, Jian, et al.

Positive shift			
Gene	Shift (°C)	pVal	Description
NUDT2	7.3	2.6E-15	Bis(5'nucleosyl)tetraphosphatase
SMU1	6.6	1.6E-09	DNA replication regulator and spliceosomal factor
CRLF3	6.6	1.6E-09	Cytokine receptor like factor 3
SYMPK	5.2	4.1E-08	Symplekin scaffold protein
GRHPR	4.7	8.5E-07	glyoxylate and hydroxypyruvate reductase
PRKAR1A	4.5	4.5E-06	PKA regulatory subunit
HEBP1	3.9	7.7E-05	Heme binding protein
OSGEP	3.7	0.00025	O-Sialoglycoprotein Endopeptidase
CERCAM	4.1	0.00050	Cerebral Endothelial Cell Adhesion Molecule
GMEB2	7.4	0.0033	Glucocorticoid Modulatory Element Binding Protein2
MAPK9	7.1	0.0063	Mitogen-activated protein kinase 9 - *JNK2*
GIPC1	2.7	0.014	PDZ domain-containing scaffolding protein
EIF3J	3.8	0.014	Eukaryotic translation initiation factor 3 subunit J
MICALL1	3.8	0.014	RAB effector
SCAF8	3.2	0.019	SR-related CTD associated factor 8, an anti-terminator
ATPAF2	2.6	0.020	ATP Synthase Mitochondrial F1 Complex Assembly Factor 2
KLHL7	3.2	0.021	Kelch-like protein 7, regulator of nucleolus
RRAGA	3.6	0.025	Ras Related GTP Binding A
DPH2	3.5	0.038	Diphthamide Biosynthesis 2
GFM1	2.6	0.038	mitochondrial translation elongation factor G1
Negative shift			
Gene	Shift (°C)	pVal	
HABP4	-10.2	1.4E-27	RNA-binding protein
HSP90AB4P	-10.1	1.2E-11	heat shock protein 90 alpha family class B member 4, pseudogene
CTDP1	-6.5	1.2E-11	phosphatase specific for the CTD of POLR2A
IRF8	-9.4	5.1E-09	Interferon Regulatory Factor 8-transcription factor
SON	-9.0	2.4E-08	DNA and RNA binding protein
PAPOLA	-7.6	1.5E-07	Poly(A) Polymerase Alpha
RNF2	-7.4	4.7E-07	E3 ligase for p53 degradation
THOC2	-7.4	4.5E-06	THO Complex 2, release of mRNA from nuclear speckles
MEF2D	-7.5	7.2E-06	Myocyte Enhancer Factor 2D
POLR1F	-6.2	7.1E-05	RNA Polymerase
DERA	-3.7	0.00046	deoxyribose phosphate aldolase
PRPF6	-6.2	0.00049	Pre-MRNA Processing Factor 6
RPL29	-6.2	0.00049	60S ribosomal protein L29, also binds heparin
POLR3A	-3.6	0.00051	largest subunit of RNA polymerase III. RNA polymerase III
LIMS4	-5.4	0.0013	LIM zinc finger domain containing 4
SMARCA5	-7.1	0.0020	SWI/SNF-related matrix-associated actin-dependent regulator of chromatin subfamily A member 5
PNN	-5.2	0.0027	Pinin
MBNL1	-6.9	0.0034	Muscleblind Like Splicing Regulator 1
WBP11	-5.6	0.0034	WW binding protein 11 splicing factor
KLF18	-4.6	0.015	Kruppel Like Factor 18
BPHL	-4.5	0.019	Biphenyl Hydrolase Like
ERO1A	-2.7	0.021	Endoplasmic Reticulum Oxidoreductase 1 Alpha
EIF3G	-4.8	0.027	Eukaryotic Translation Initiation Factor 3 Subunit G
GNL2	-4.7	0.031	Nucleolar GTP-binding protein 2
RPL31	-5.9	0.038	Ribosomal Protein L31

Supplemental Table S1. Cellular Thermal Shift Assay screen for proteins that bind NAV-2729. RD cell lysates were mixed with DMSO or 50 μM NAV-2729 and subjected to a temperature

ramp. The lysates were centrifuged and the proteins remaining in solution were detected by mass spectrometry. The data were then analyzed to determine temperature shifts as described in "Materials and Methods." 19 of the 25 proteins determined to have a significant negative temperature shift bound to nucleotide or nucleic acid. 8 of 20 with a positive shift bound to nucleotide or nucleic acid.